Space Vector Modulation of Dual Inverter Motor Drive Compared with Single Inverter Drive

Melinda B. Fauziah, Yoshiaki Oto and Toshihiko Noguchi
Shizuoka University, Japan

Abstract. This paper describes space vector modulation (SVM) techniques for different motor drive systems. Two three-phase topologies are compared from the viewpoints of switching sequences and the resultant voltage waveforms, i.e., an open-end winding motor fed by dual inverters and a conventional star-connected three-winding motor fed by a single inverter. In the dual inverter system, both the inverters are supplied by batteries with a 1:1 DC-bus voltage ratio, while in the single inverter system, the DC-DC converter is employed to supply the inverter. The simulation results compared with the single inverter system show that, with the identical motor speed command value, the dual inverter motor drive system can generate 9-level voltage waveforms which can suppress the total harmonic distortion (THD) of the voltage down to 35.86% and THD of the current down to 6.39%.

1. Introduction

The increasing number of transportations on the road have led to the significant increase in the amount of carbon dioxide emissions. This is one of the considerations intensively focused on the whole world as well as Japan. In particular, hybrid electric vehicles are being utilized and the manufactures have a task in developing technology in order to reduce the amount of the carbon dioxide emissions. Nowadays, many of the hybrid electric vehicles employ three-phase permanent magnet (PM) motors driven by a combination of a DC-DC converter and a three-phase two-level inverter. However, this system generates three-level voltage waveforms with a high dv/dt which cause increase of harmonics in the output voltage waveforms [1] [2]. This condition can reduce the motor efficiency and can cause electromagnetic interference (EMI) [3] [4]. To solve these problems, an open-end winding motor fed by dual inverters has been examined in this research [5]-[10].

This paper presents both the single and the dual inverter motor drive systems which can be employed in the hybrid electric vehicles. The computer simulations have been conducted to confirm the performance of both systems, especially, regarding the reduction of the THD.

2. Principles of Single Inverter and Dual Inverter System

2.1. Circuit Configurations and SVM

The conventional system consisting of a three-phase PM motor driven by a combination of a DC step-up converter and a two-level inverter is depicted in Fig. 1. The voltage boosted by the DC-DC converter is operated as the input of the inverter and the three windings of the motor are connected to a neutral point. On the other hand, in the open-end winding motor, the neutral point is opened, and two inverters feed the windings from each end as shown in Fig. 2. In the dual inverter system, the inverter on the left side is called INV1 and the other is INV2. Each leg of INV1 and INV2 is operated complementary.
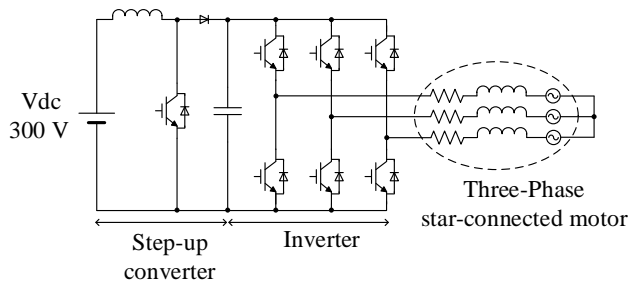
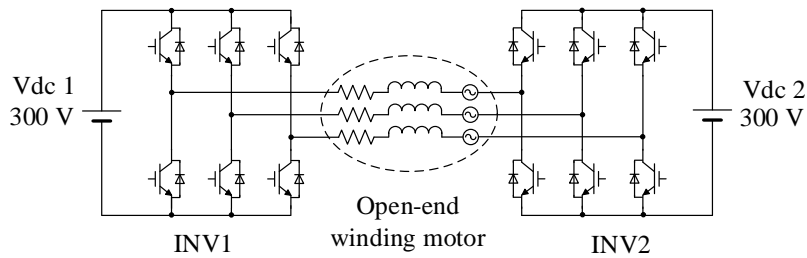**Fig. 1.** Conventional motor drive system.

Fig. 2. Open-end winding motor fed by dual inverter.

Fig. 3 shows the space voltage vectors which consist of the output voltage vectors in the cases of the single inverter and the dual inverter. As can be seen in Fig. 3 (a), the single inverter can generate 8 voltage vectors, i.e., 6 non-zero vectors and 2 zero vectors. The output voltage vectors generated by the dual inverter are the summing result of the basic voltage vectors of INV1 and INV2. Fig. 3 (b) is the voltage vectors generated by the dual inverter with the battery-battery system in which both DC-buses are supplied by batteries with a 1:1 DC-bus voltage ratio.

(a) Single inverter.

(b) 1:1 DC-bus voltage ratio in dual inverter.

Fig. 3. Space voltage vectors.

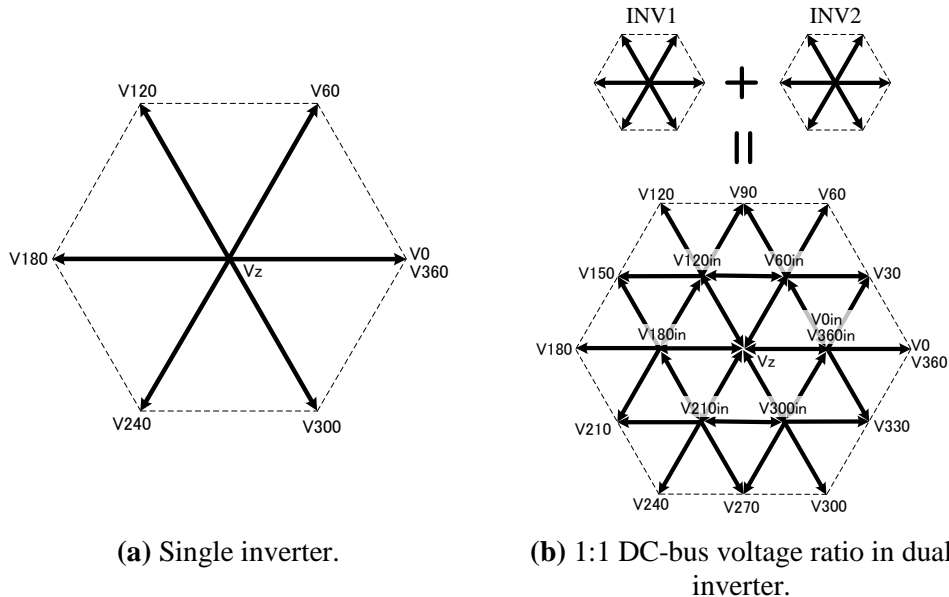Fig. 4 shows the expanded space voltage vectors of both the single inverter and the dual inverter system in the electrical angle range of 0 to 60 deg. The binary numbers represent the ON-OFF states of each inverter leg where the value 1 indicates that the upper transistor is turned on whereas the value 0 indicates that the lower transistor is turned on. For the single inverter, the corresponding

combinations of the switching states are shown in brackets as depicted in Fig. 4 (a). Since the dual inverter is composed of the two voltage sources, the corresponding combinations of the switching states represented by ( ) and ( )' indicate the voltage vectors of INV1 and INV2, respectively, as shown in Fig. 4 (b). The voltage vectors can be obtained by multiple switching states having a specific magnitude and a phase angle. This means that the dual inverter has switching state redundancy which provides flexibility to generate multilevel voltage waveforms.
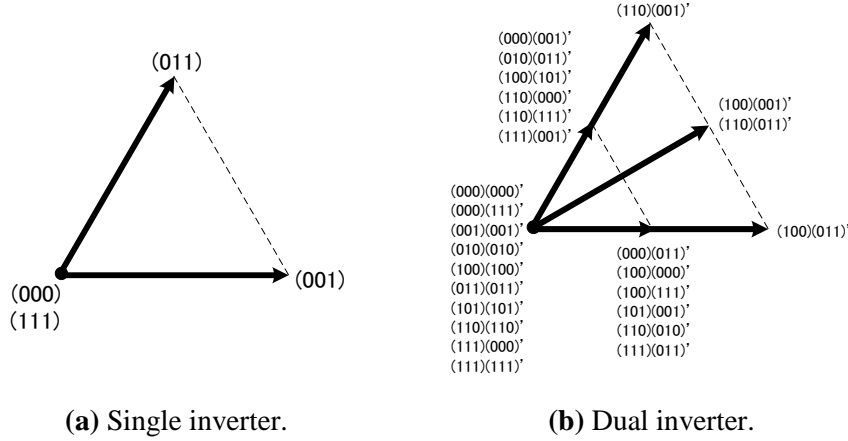

(a) Single inverter.　　　　**(b)** Dual inverter.

Fig. 4. Switching states.

2.2. Sector Identification

The sector of the single inverter is identified, regarding the value of the phase angle in which each sector has 60-deg difference. For instance, the sector from 0 to 60 deg is called sector 1, the next 60 deg is sector 2, and so on. In the case of the dual inverter system, the sector identification is proposed by using the space voltage vectors as shown in Fig. 5. The hexagon is divided into 6 regions with 60-deg phase zone in which each region is also divided into 4 equilateral triangle sectors. The region from 0 to 60 deg is called region 1 and the sectors located in region 1 are sector #11, #12, #13, and #14. Boundary lines, which are a, b, c, d, e, and f limiting the sectors, are employed to identify the location of the reference voltage vector.

Overall boundary line equations :

$$a : V_\beta = \frac{1}{4}\sqrt{2} \qquad\qquad d : V_\beta = -\sqrt{3}V_\alpha + \frac{1}{2}\sqrt{2}$$

$$b : V_\beta = \sqrt{3}V_\alpha - \frac{1}{2}\sqrt{2} \qquad e : V_\beta = -\sqrt{3}V_\alpha - \frac{1}{2}\sqrt{2}$$

$$c : V_\beta = \sqrt{3}V_\alpha + \frac{1}{2}\sqrt{2} \qquad f : V_\beta = -\frac{1}{4}\sqrt{2}$$

$$V_\beta \leq \frac{1}{4}\sqrt{2}$$

$$V_\beta \leq \sqrt{3}V_\alpha - \frac{1}{2}\sqrt{2}$$

$$V_\beta \geq -\sqrt{3}V_\alpha + \frac{1}{2}\sqrt{2}$$

(a) Division of sector location.　　　　**(b)** Sector identification approach.
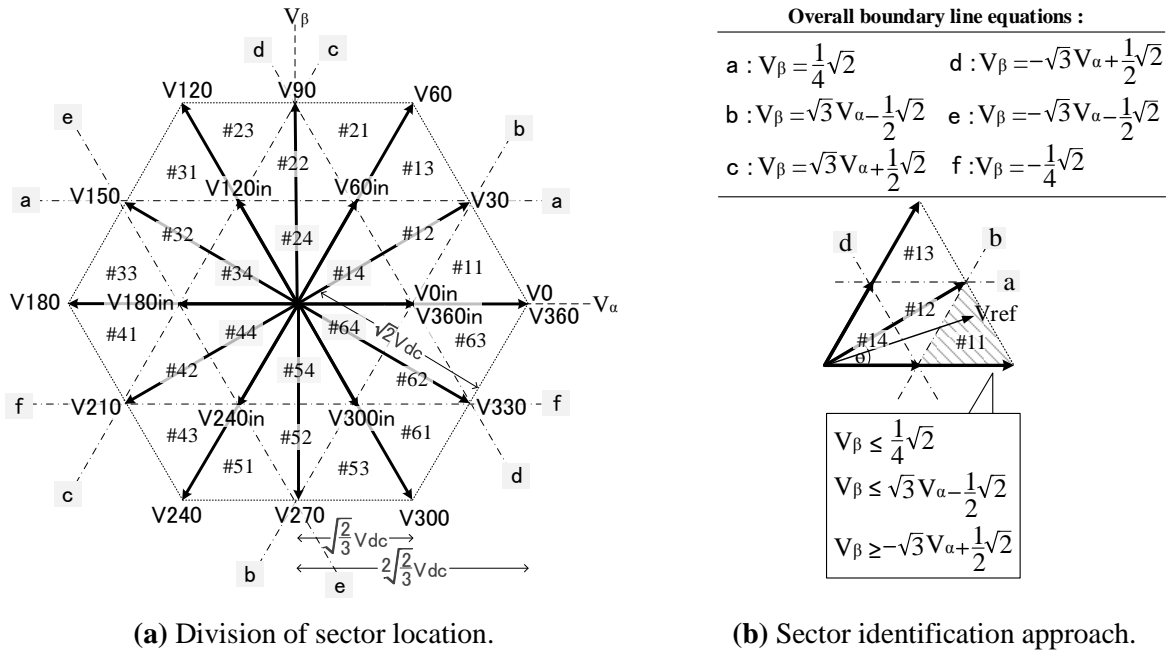
Fig. 5. Proposed sector identification in dual inverter system.

The equation of each boundary line can be calculated by considering the maximum voltage vector amplitude and the reference voltage vector decomposed into αβ-axis. The maximum voltage vector amplitude can be obtained as follows:

$$|V_0| = |V_{60}| = |V_{120}| = |V_{180}| = |V_{240}| = |V_{300}| = |V_{360}| = 2\sqrt{\frac{2}{3}}V_{dc}, \tag{1}$$

$$|V_{30}| = |V_{90}| = |V_{150}| = |V_{210}| = |V_{270}| = |V_{330}| = \sqrt{2}V_{dc}, \text{ and} \tag{2}$$

$$|V_{0in}| = |V_{60in}| = |V_{120in}| = |V_{180in}| = |V_{240in}| = |V_{300in}| = |V_{360in}| = \sqrt{\frac{2}{3}}V_{dc}, \tag{3}$$

where V_{dc} is equal to $V_{dc1} = V_{dc2}$, $V_0 \ldots V_{360}$ are large vectors, $V_{30} \ldots V_{330}$ are medium vectors, and $V_{0in} \ldots V_{360in}$ are small vectors having a half magnitude of the large vector. Moreover, the voltage vector can be calculated as follows:

$$V_{ref} = \frac{V_\alpha}{\cos\theta} = \frac{V_\beta}{\sin\theta}, \tag{4}$$

where V_{ref} is a reference voltage vector, V_α and V_β are voltage vectors decomposed into αβ-axis, and θ is a space vector angle. The overall line equations are presented in Fig. 5 (a). For instance, if the reference voltage vector is located in the sector #11, boundary line equations a, b, and d are required. The sector can be selected using inequality equations of the boundary lines as shown in Fig. 5 (b).

If the position of the reference voltage vector has been determined, the three voltage vectors surrounding the corresponding sector are employed to generate the reference voltage vector. For instance, if sector #11 is detected, V_{0in}, V_0, and V_{30} are employed to generate the reference voltage vector.

2.3. Switching State

The switching states in a SVM period should assure the symmetrical output voltage pulse sequence to improve the THD and to reduce the switching losses. It is necessary to arrange the switching state sequence in which during the transition of one switching state to the next one, only one leg is switched over. Therefore, during 1 period, the appropriate switching states which are selected to achieve the symmetrical voltage waveform both in the single and in the dual inverter system are depicted in Fig. 6. In the case of the single inverter system, for instance, when the reference voltage vector is in sector #1, the sequence of the switching states shown in Fig. 6 is selected. In the sector #11 of the dual inverter system, since all are non-zero vectors, the sequence of switching states is determined by choosing the least transition.
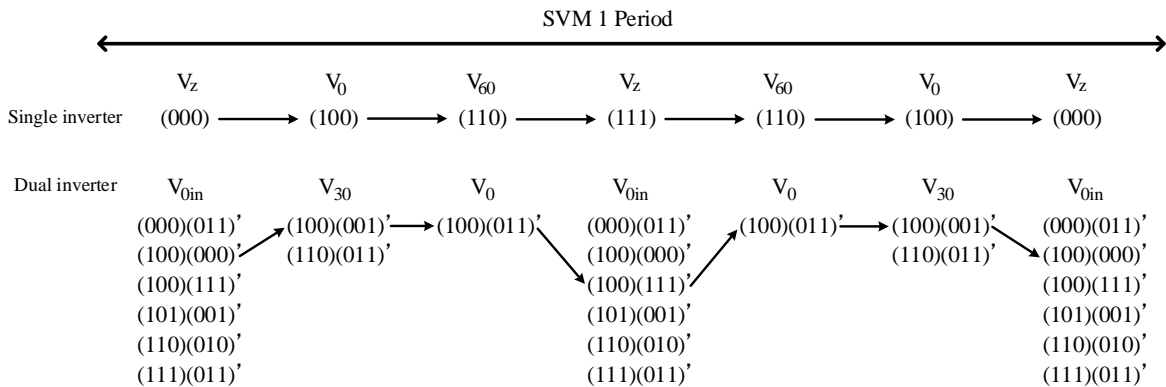

Fig. 6. Appropriate switching states selected to achieve symmetrical voltage patterns.
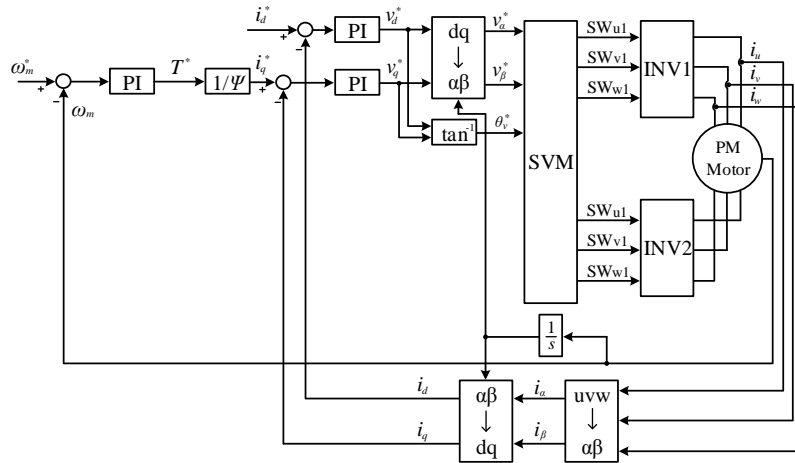
3. Simulation and Result

The computer simulations have been conducted to observe the operation waveforms of the space vector modulation in single inverter and the dual inverter system. The overall block diagrams of the single inverter and the dual inverter systems are shown in Fig. 10 and 11, respectively. A vector control algorithm is utilized to control the motor in which closed-loop current controllers and a speed controller are used to improve the performance.

The simulation is examined based on the condition and the motor parameters as shown in Table 1. The simulation results are motor rotation speed, U-phase voltage and three-phase currents for both the single inverter and the dual inverter depicted in Fig. 9 (a) and (b), respectively. THD of the voltage and the current has also been measured in each system. From both simulation results, the performance of the motor rotation speed can reach the command value at 5000 r/min. By examining the U-phase voltage of the motor windings, the 5-level voltage waveform can be achieved in the single inverter system and the 9-level voltage waveform can be achieved in the dual inverter system. Three phase-currents of the single and the dual inverter system show sinusoidal waveforms. Compared Fig. 9 (a) with (b), it can be found that the THDs of the voltage and the current are significantly reduced. The dual inverter system can generate more voltage levels and can create smoother waveforms than those of the single inverter system. Moreover, phase current waveforms of the single inverter have many harmonics, compared with the dual inverter system.

Table 1. Simulation conditions and parameters.

DC-DC converter parameters	Inductor	75 μH
	Capacitor	67 μF
	Duty Cycle	0.5
	Switching frequency of Converter	25 kHz
	Input Voltage of Converter	300 V
Inverter parameters	Switching frequency of Inverter	10 kHz
	Voltage of battery (INV1 and INV2)	300 V
	Dead time	0 μs
Motor parameters	Motor speed command value	5000 r/min
	Number of poles	4
	Number of flux linkage	0.1 Wb
	Moment of inertia	0.0001 kgm^2
	Damping coefficient	0.002 N/rad/s
	Phase resistance	1 Ω
	Phase inductance	5 mH

Fig. 7. Block diagram of PM motor drive fed by single inverter system.

Fig. 8. Block diagram of open-end winding PM motor drive fed by dual inverter system.

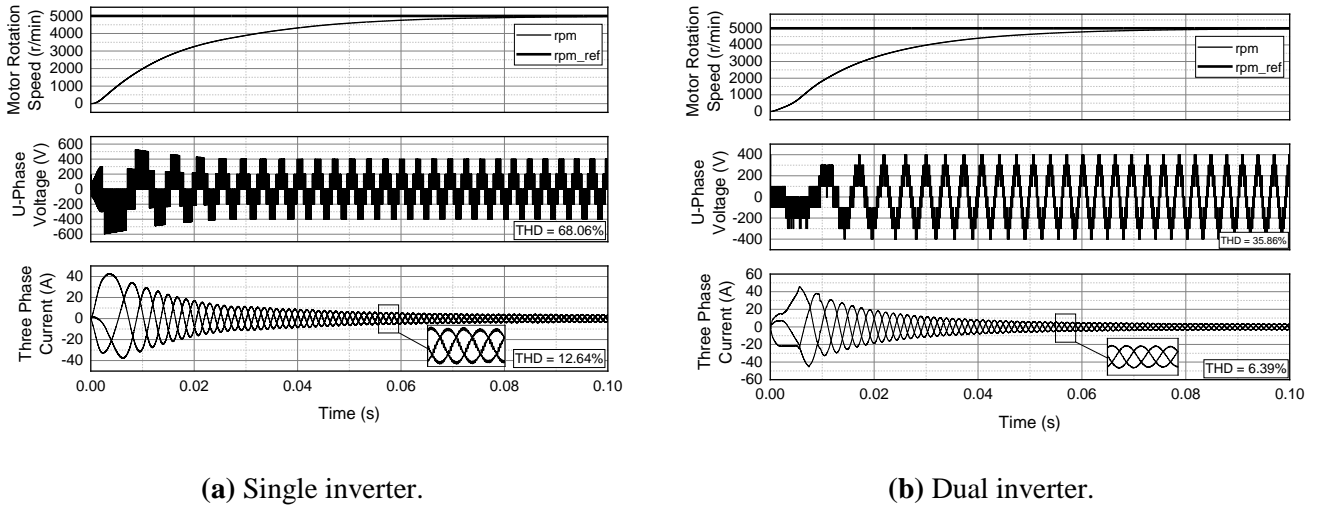**(a)** Single inverter.　　　　**(b)** Dual inverter.

Fig. 9. Simulation results.

4. Conclusion

The simulations of the single and the dual inverter motor drive systems have been presented. In the dual inverter system, the sector identification is determined by using the approach of the boundary line equations. The selection of the appropriate switching states in the dual inverter among the redundancy must be considered regarding the switching losses. The simulation results show that, with the identical motor speed command value, the dual inverter motor drive system can generate 9-level voltage waveforms which can suppress the THD of voltage down to 35.86% and the THD of the current down to 6.39%. Therefore, it can be concluded that it is beneficial to use the open-end winding motor fed by the dual inverter employed in the hybrid electric vehicles.

References
[1] Y. Ohto, T. Noguchi, and T. Sasaya, "Space Vector Modulation of Dual Inverter with Battery and Capacitor across DC Buses," *IEEE International Conference on Power Electronics and Drive System*, 2017, 1172-1177.
[2] K. Mitsudome, H. Haga, and S. Kondo, "Improvement of Output Voltage Waveform in Dual Inverter Having a Different DC Power Supply," *IEEJ Technical Meeting on Rotating Machinery, Semiconductor Power Converter and Motor Drive,* 2015, pp. 77-82.

[3] J. Ewanchuk, J. Salmon, and C. Chapelsky, "A Method for Supply Voltage Boosting in an Open-Ended Induction Machine Using a Dual Inverter System With a Floating Capacitor Bridge," *IEEJ Transactions on Power Electronics,* vol. 28, no. 3, 2013, pp. 1348-1357.

[4] Q. An, J. Liu, Z. Peng, L. Sun, and L. Sun, "Dual-Space Vector of Open-End Winding Permanent Magnet Synchronous Motor Drive Fed by Dual Inverter," *IEEE Transactions of Power Electronics,* vol. 31, 2016, pp. 8329-8342.

[5] P. Sandulescu, F. Meinguet, X. Kestelyn, E. Semail, and A. Bruyere, "Control Strategies for open-end winding drives operating in the flux-weakening region," *IEEE Transactions of Power Electronics,* vol. 29, no. 9, 2014, pp. 4829-4842.

[6] S. Jain, A.K. Thopukara, R. Karampuri, and V.T. Somasekhar, "A Single-Stage Photovoltaic System for a Dual-Inverter-Fed Open-End Winding Induction Motor Drive for Pumping Applications," *IEEE Transactions of Power Electronics,* vol. 30, no. 9, 2015, pp. 4809-4818.

[7] S. Srinivas, and K.R. Sekhar, "Theoretical and Experimental Analysis for Curreent in a Dual-Inverter-Fed Open-End Winding Induction Motor Drive With Reduced Switching PWM," *IEEE Transactions on Industrial Electronics,* vol. 60, no. 10, 2012, pp. 4318-4328.

[8] A. Amerise, M. Mengoni, L. Zarri, A. Tani, S. Rubino, and R. Bojoi, "Open-End Windings Induction Motor Drive With Floating Capacitor Bridge at Variable DC-Link Voltage," *IEEE Transactions on Industry Applications,* vol. 55, no. 3, 2019, pp. 2741-2749.

[9] S. Foti, S.D. Caro, G. Scelba, T. Scimone, A. Testa, M. Cacciato, and G. Scarcella, "An Optimal Current Control Strategy for Asymmetrical Hybrid Multilevel Inverters," *IEEE Transactions on Industry Applications,* vol. 54, no. 5, 2018, pp. 4425-4436.

[10] B.R. Vinod, M.R. Baiju, and G. Shiny, "Five-Level Inverter-Fed Space Vector Based Direct Torque Control of Open-End Winding Induction Motor Drive," *IEEE Transactions on Energy Conversion,* vol. 33, no. 3, 2018, pp. 1392-1401.